*polymers*

MDPI

*Article*

# Radiation Attenuation Calculation of 3D-Printed Polymers Across Variable Infill Densities and Phase Angles for Nuclear Medicine Applications

**Toni Beth Lopez [1,2,*], James Harold Cabalhug [1], Emmanuel Arriola [1,3], Marynella Laica Afable [1], Ranier Jude Wendell Lorenzo [1], Glenn Bryan Fronda [1], Patrick Mecarandayo [1], Gil Nonato Santos [2], Rigoberto Advincula [4], Alvie Astronomo [5] and Michael Joe Alvarez [6]**

1 Department of Science and Technology, Metals Industry Research and Development Center, Taguig City 1631, Philippines; jpcabalhug@gmail.com (J.H.C.); erarriola@mirdc.dost.gov.ph (E.A.); afablemarynella@gmail.com (M.L.A.); lorenzoranier@gmail.com (R.J.W.L.); glennfronda190@gmail.com (G.B.F.); pamecarandayo@mirdc.dost.gov.ph (P.M.)
2 Department of Physics, De La Salle University, Manila 0922, Philippines; gil.santos@dlsu.edu.ph
3 Department of Mechanical Engineering, De La Salle University, Manila 0922, Philippines
4 Department of Chemical and Biomolecular Engineering, University of Tennessee, Knoxville, TN 37996, USA; rca41@case.edu
5 Department of Science and Technology, Philippine Nuclear Research Institute, Quezon City 1101, Philippines; ajasuncion@pnri.dost.gov.ph
6 St. Elizabeth Hospital, Inc., General Santos City 9500, Philippines; msalvarez@sehi.ph
* Correspondence: tblopez@mirdc.dost.gov.ph

## Abstract

This study investigates the modulation effects of varying infill densities and phase angles on the radiation attenuation properties of three 3D-printed polymers: acrylonitrile butadiene styrene (ABS), polylactic acid (PLA), and thermoplastic polyurethane (TPU). Using the EpiXS software for radiation attenuation calculations, the study assessed the linear attenuation coefficients (LACs) of the materials under different infill densities (30%, 50%, 70%, 90%, and 100%) and phase angles (0°, 30°, 45°, 60°, and 90°) for radiation in the 1–100 keV energy range, which corresponds to the X-ray spectrum. TPU demonstrated the highest attenuation values, with a baseline coefficient of 20.199 $cm^{-1}$ at 30% infill density, followed by PLA at 18.835 $cm^{-1}$, and ABS at 13.073 $cm^{-1}$. Statistical analysis via the Kruskal–Wallis test confirmed that infill density significantly impacts attenuation, while phase angle exhibited no significant effect, with *p*-values exceeding 0.05 across all materials. TPU showed the highest sensitivity to infill density, with a slope of 1.1194, compared to 0.7257 for ABS and 0.9251 for PLA, making TPU the most suitable candidate for radiation protection applications, particularly in applications where flexibility and high attenuation are required. The findings support the potential of 3D printing to produce customized, cost-effective radiation protection gear for medical and industrial applications. Future work can further optimize material designs by exploring more complex infill geometries and testing under broader radiation spectra.

**Keywords:** additive manufacturing; linear attenuation coefficient; PLA; TPU; ABS

Check for updates

Academic Editors: Sayan Ganguly, Sagar Umesh Patil and Sagar Shah

Received: 30 October 2025
Revised: 15 December 2025
Accepted: 18 December 2025
Published: 24 December 2025

**Copyright:** © 2025 by the authors. Licensee MDPI, Basel, Switzerland. This article is an open access article distributed under the terms and conditions of the Creative Commons Attribution (CC BY) license.

## 1. Introduction

The use of ionizing radiation in medical treatments has been highly effective in treating various forms of cancer, but it also presents inherent risks, especially to healthcare

practitioners. Professionals consistently exposed to radiation over extended periods are at increased risk of developing radiation-induced health issues, including both acute and chronic conditions. Studies have shown that radiation exposure can result in a spectrum of health effects, ranging from mild radiation sickness to severe illnesses such as cancer. Long-term exposure has even been linked to fatalities in some instances [1–4].

Global health reports indicate that over 1000 healthcare professionals worldwide experience significant radiation exposure annually, underscoring the urgent need for more effective protective measures [3,5]. Despite the clear risks, the prohibitive cost of radiation shielding equipment remains a challenge. Modern radiation protective gear can cost from USD 43 (per piece) to USD 602 (per set), making accessibility difficult for many institutions [6]. As both healthcare workers and patients undergoing radiation therapy or diagnostic procedures face these risks, the scientific community has focused on developing lightweight, wearer-specific, and cost-effective radiation protection gear to mitigate exposure and improve safety [7–11].

Additive manufacturing, particularly 3D printing, has emerged as a promising solution for addressing these challenges in radiation protection [12,13]. Unlike traditional manufacturing methods, 3D printing allows for the creation of custom-fitted radiation treatment aids, such as boluses, which can be tailored to the patient's anatomy [5,14,15]. This approach enhances treatment accuracy by ensuring that the radiation dose is delivered precisely to the targeted areas, minimizing unnecessary exposure to surrounding tissues. Furthermore, fitted designs are crucial not only for patient safety but also for the medical staff, whose protective gear must offer both comfort and adequate shielding. In contrast to commercially available radiation protection garments, which are often bulky and ill-fitting, 3D-printed, patient-specific designs offer significant advantages in both protection and comfort [5,14].

While material-based improvements, such as incorporating tungsten, bismuth, or lead alternatives, have been the dominant focus of recent studies, geometry-driven approaches remain underexplored—particularly those leveraging standard, commercially available thermoplastics without chemical modification. In this context, the present study introduces a novel strategy for modulating X-ray attenuation through variations in infill density and phase angle, enabling a non-chemical, structure-dependent means of enhancing radiological performance using commonly accessible FDM materials. The selected polymers—ABS, PLA, and TPU—represent three distinct classes of engineering thermoplastics (rigid, semi-rigid, and flexible, respectively) [16,17] and are among the most widely used materials in 3D printing. Their differences in intrinsic density, structural composition, and mechanical behavior provide a meaningful basis for evaluating how polymer characteristics interact with internal geometry to influence photon attenuation [16–18].

The growing literature in radiotherapy and medical imaging demonstrates that additive manufacturing has become increasingly relevant for producing patient-specific boluses and anatomical phantoms that improve dose conformity through precise anatomical matching. Recent studies have begun to establish the scientific relevance of structural parameters in influencing radiation–material behavior. Ciobanu et al. (2024) highlighted that filament density directly affects the dosimetric absorbance of high-energy photons to 3D-printed bolus materials, which mimics the human tissue [19]. Similarly, Kavun and Kamer (2026) demonstrated that variations in the line width and layer height alter the shielding performance of 3D-printed PLA, confirming that even subtle changes in printing architecture can influence attenuation [20]. Advances in 3D-printed phantoms further reinforce this trend; Mei et al. (2023) successfully fabricated pixel-like soft tissue and bone phantoms whose tunable Hounsfield Units were achieved by manipulating infill configurations, illustrating the capacity of AM to deliver geometrically customized radiation responses [21].

Despite these developments, most state-of-the-art studies continue to rely on modifying base materials through high-Z fillers or composite formulations to achieve greater attenuation. Although effective, such approaches introduce additional cost, regulatory hurdles, and material safety qualification requirements that may delay clinical translation. By contrast, the systematic exploration of intrinsic AM tunability, i.e., particularly through infill density and internal geometric architecture, remains limited, even though these parameters are readily adjustable within standard FDM workflows and require no modification of the polymer chemistry. This gap is significant because structural manipulation offers an accessible, repeatable, and clinically translatable means of tailoring the radiological behavior of widely used and commercially available thermoplastics such as PLA, ABS, and TPU.

The emerging shift toward calculation-based pre-optimization further underscores the timeliness of this work. Studies demonstrating structure-dependent attenuation have motivated the use of validated photon interaction databases and software tools to predict material performance before committing to fabrication. Building on this direction, the present study quantifies how the linear attenuation coefficient can be tailored solely through modifications in infill-related design parameters. This approach provides a practical, material-agnostic pathway for enhancing bolus and phantom performance in radiotherapy, ensuring accessibility and reproducibility while remaining aligned with standard clinical and manufacturing practices.

It is important to note that intrinsic densities reported by manufacturers may not match the effective density of printed parts, because printing parameters (e.g., extrusion temperature, cooling rate, bed temperature, cooling-fan speed, flow rate) influence polymer microstructure—notably crystallinity and porosity—as well as interlayer adhesion and void formation. For example, in semi-crystalline materials such as PLA, 3D-printing deposition parameters have been shown to produce crystallinity ranging from ~14% up to ~71% depending on thermal history and cooling conditions [18]. Such variation in crystallinity (and associated porosity/interlayer fusion) significantly affects the effective density, mechanical, and thermal behavior of the printed parts [22]. For amorphous (e.g., ABS) or elastomeric (e.g., TPU) polymers, while crystallinity changes may be less relevant, density deviations relative to nominal bulk values may still occur due to differences in interlayer bonding, packing efficiency, void content, and layer orientation—factors well known to influence FDM print quality and part density [23]. Hence, while our computational analysis relies on manufacturer-reported densities, we explicitly acknowledge that actual printed parts may differ substantially because of microstructural and process-driven effects.

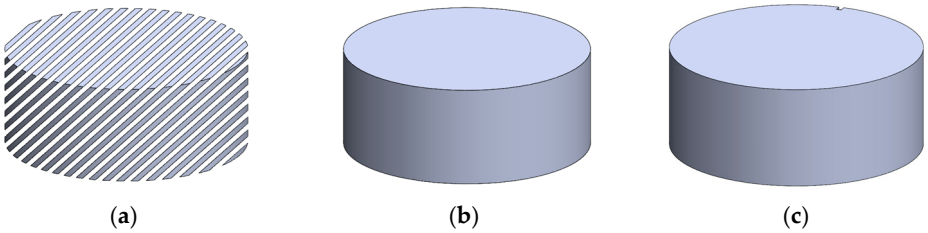
The integration of additive manufacturing into the production of radiation protection equipment offers significant potential to reduce costs, improve the effectiveness of radiotherapy treatments, and increase the safety of healthcare professionals. By utilizing advanced materials and innovative design techniques, 3D printing can overcome the limitations of traditional radiation shielding gear, paving the way for more efficient and accessible solutions in radiotherapy. This study seeks to design and develop radiation protective gear by employing 3D printing technology, specifically varying infill densities and phase angles, to optimize radiation attenuation.

## 2. Materials and Methods

The study implementation was subdivided into Computer-Aided Design (CAD) [24] and density calculation, radiation attenuation calculation [25], and statistical analysis of attenuation effects.

### *2.1. Computer-Aided Design (CAD) and Theoretical Density Calculation*

The design of the test specimens for the irradiation tests was generated using CAD software, Dassault SolidWorks version 2020 [26]. The sample is a cylinder-shaped block with 50 mm in diameter and 20 mm in height; see Figure 1. The wall and infill thicknesses are both two (2) millimeters. The infill was modeled first using an extruded boss/base command, then extruded cut for the profile of the cylinder. Lastly, the shell of the specimen was created using the *extrude-thin* command.



(**a**) (**b**) (**c**)

**Figure 1.** Modeling of the Test Specimen (**a**) infill design, (**b**) with walls, and (**c**) with walls and slot feature.

Based on the design of the experiment presented in the previous subsection, the distance between infills is shown in Figure 2. Computed distances are presented in Table 1. A configuration table was used to easily produce CAD models with varying properties in a single "*.sldprt*" file.

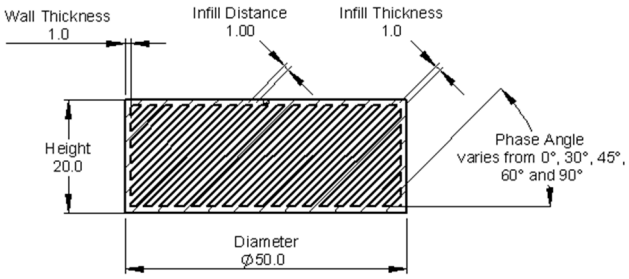



**Figure 2.** Test Specimen Design.

**Table 1.** Summary of Infill Densities.

| Infill Density, % | Distance of Infills, mm |
|---|---|
| 30 | 2.33 |
| 50 | 1.00 |
| 70 | 0.44 |
| 90 | 0.11 |
| 100 | - |

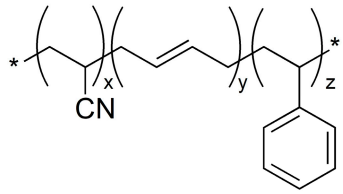
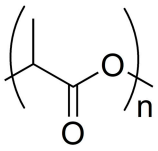
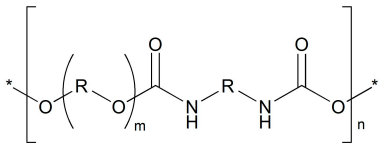
The densities of ABS, PLA, and TPU were obtained from the manufacturers' datasheets. The relative densities of the materials were then calculated, accounting for the air gaps within the infill structure, which effectively reduced the overall mass of the samples. Using CAD software, the volume of the infill was determined, and from this, the relative mass of each sample was computed. Given that the sample was enclosed by a solid outer wall, the total volume was fixed at 39.25 $cm^3$, corresponding to a cylindrical geometry.

### *2.2. Radiation Attenuation Calculation*

The attenuation modulation of ABS, PLA, and TPU was investigated using EpiXS software 2021 version developed by the DOST—Philippine Nuclear Research Institution

(PNRI) [25]. This free software requires a Windows operating system and can be downloaded through its official website. This study utilized the EPICS2017 (ENDF/B-VIII) photolibrary. The linear attenuation coefficient was extracted from the software by inputting the calculated densities from CAD. Chemical formulas of ABS, PLA, and TPU were also included in the calculation parameter, as well as the colorant, which is the titanium dioxide ($TiO_2$). In the EpiXS program, the calculation parameter selected was dependent on the percent concentration of the compounds and the material is considered a mixture. The concentration was based on the manufacturer's datasheet with the following concentrations: ABS (98%):$TiO_2$ (2%); PLA (99.8%):$TiO_2$ (0.2%); and TPU (99%):$TiO_2$ (1%). To have a uniform comparison, the color selection is limited to white (Table 2).

**Table 2.** Polymer structure and its corresponding characteristics.

| Polymer | Chemical Formula | Chemical Structure | Characteristics | References |
|---|---|---|---|---|
| ABS | $((C_8H_8 \cdot C_4H_6 \cdot C_3H_3N)_n)$ |  | Tensile strength at break is 15–50 MPa; strong, stiff, and durable; chemically resistant material; resistant to warping; 1.03 g/cc density | [27] |
| PLA | $((C_3H_4O_2)_n)$ |  | Tensile strength at break is 31–43 MPa; Very brittle; easy to print; non-toxic; and biodegradable; 1.24 g/cc density | [28] |
| TPU | $((C_3H_8N_2O)_n)$ |  | Tensile strength at break is 22–40 MPa; adoption to medical applications; high ductility and toughness; 1.22 g/cc density | [29,30] |

* denotes the connection points where the repeating units occur.

### *2.3. Statistical Analysis of Linear Attenuation Coefficients*

Varying the infill density and phase angles imposed varying linear attenuation coefficients. These differences were statistically analyzed using the non-parametric Kruskal–Wallis test and regression analysis through Python 3.12.7/Jupyter Notebook (jupyterlab 4.2.5). The statistical analysis provided insights into the modulation effect of varying the infill densities and phase angles of different polymers for the X-ray radiation region.

## 3. Results and Discussion

The main advantage of 3D printing in designing radiation protective gears allows the introduction of airgaps in a uniform pattern. From Table 3, the gray areas represent the 3D printed and the black ones represent the airgaps. Phase angle orientation is based on the +*x*-axis as zero angle and in a counterclockwise direction. Based on the CAD models, with the increasing infill density, the airgaps were uniformly minimized.

The relative densities of each sample were determined by calculating the volumes using Computer-Aided Design (CAD) software. These calculations provided the total volume of the 3D-printed parts, including both the solid material and any air gaps present in the infill structure. The calculated volumes, detailed in Table 4, allowed for the computation of the relative densities by dividing the measured mass of each sample by its corresponding volume. This method provided a more accurate representation of the material's density,

accounting for variations in infill patterns and the introduction of air gaps, which can significantly impact the overall density of the printed parts.

**Table 3.** CAD designs of varying infill densities and phase angles.

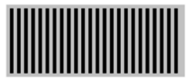
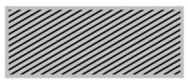
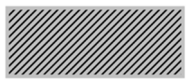
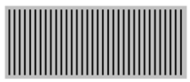
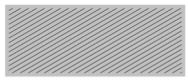
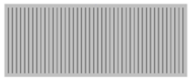
| Infill Density (%) | Angle | | | | |
|---|---|---|---|---|---|
| | 0° | 30° | 45° | 60° | 90° |
| 30% |  |  |  |  |  |
| 50% |  |  |  |  |  |
| 70% |  |  |  |  |  |
| 90% |  |  |  |  |  |

**Table 4.** Summary of Theoretical Densities of Varying Infill Density and Phase Angle of ABS, PLA, and TPU.

| Material | Infill Density | Infill Phase Angle | Theoretical Volume with Airgap, $cm^3$ | Theoretical Volume of Infill, $cm^3$ | Theoretical Mass, g | Theoretical Density, $g/cm^3$ |
|---|---|---|---|---|---|---|
| ABS | 30 | 0 | 39.25 | 15.746 | 17.64 | 0.44931 |
| ABS | 50 | 0 | 39.25 | 22.984 | 25.74 | 0.65585 |
| ABS | 70 | 0 | 39.25 | 28.815 | 32.27 | 0.82224 |
| ABS | 90 | 0 | 39.25 | 35.651 | 39.93 | 1.01730 |
| ABS | 100 | 0 | 39.25 | 39.25 | 43.96 | 1.12000 |
| PLA | 30 | 0 | 39.25 | 15.746 | 18.42 | 0.46937 |
| PLA | 50 | 0 | 39.25 | 22.984 | 26.89 | 0.68513 |
| PLA | 70 | 0 | 39.25 | 28.815 | 33.71 | 0.85894 |
| PLA | 90 | 0 | 39.25 | 35.651 | 41.71 | 1.06272 |
| PLA | 100 | 0 | 39.25 | 39.25 | 45.92 | 1.17000 |
| TPU | 30 | 0 | 39.25 | 15.746 | 19.21 | 0.48943 |
| TPU | 50 | 0 | 39.25 | 22.984 | 28.04 | 0.71441 |
| TPU | 70 | 0 | 39.25 | 28.815 | 35.15 | 0.89565 |
| TPU | 90 | 0 | 39.25 | 35.651 | 43.49 | 1.10813 |
| TPU | 100 | 0 | 39.25 | 39.25 | 47.89 | 1.22000 |
| ABS | 30 | 30 | 39.25 | 16.471 | 18.45 | 0.47000 |
| ABS | 50 | 30 | 39.25 | 22.981 | 25.74 | 0.65576 |
| ABS | 70 | 30 | 39.25 | 29.498 | 33.04 | 0.84173 |
| ABS | 90 | 30 | 39.25 | 36.013 | 40.33 | 1.02763 |
| ABS | 100 | 30 | 39.25 | 39.25 | 43.96 | 1.12000 |
| PLA | 30 | 30 | 39.25 | 16.471 | 19.27 | 0.49098 |
| PLA | 50 | 30 | 39.25 | 22.981 | 26.89 | 0.68504 |
| PLA | 70 | 30 | 39.25 | 29.498 | 34.51 | 0.87930 |
| PLA | 90 | 30 | 39.25 | 36.013 | 42.14 | 1.07351 |
| PLA | 100 | 30 | 39.25 | 39.25 | 45.92 | 1.17000 |
| TPU | 30 | 30 | 39.25 | 16.471 | 20.09 | 0.51196 |
| TPU | 50 | 30 | 39.25 | 22.981 | 28.04 | 0.71431 |
| TPU | 70 | 30 | 39.25 | 29.498 | 35.99 | 0.91688 |
| TPU | 90 | 30 | 39.25 | 36.013 | 43.94 | 1.11938 |
| TPU | 100 | 30 | 39.25 | 39.25 | 47.89 | 1.22000 |
| ABS | 30 | 0 | 39.25 | 15.746 | 17.64 | 0.44931 |

**Table 4.** *Cont.*

| Material | Infill Density | Infill Phase Angle | Theoretical Volume with Airgap, $cm^3$ | Theoretical Volume of Infill, $cm^3$ | Theoretical Mass, g | Theoretical Density, $g/cm^3$ |
|---|---|---|---|---|---|---|
| ABS | 30 | 30 | 39.25 | 16.471 | 18.45 | 0.47000 |
| ABS | 30 | 45 | 39.25 | 16.468 | 18.44 | 0.46991 |
| ABS | 30 | 60 | 39.25 | 16.474 | 18.45 | 0.47009 |
| ABS | 30 | 90 | 39.25 | 16.438 | 18.41 | 0.46906 |
| PLA | 30 | 0 | 39.25 | 15.746 | 18.42 | 0.46937 |
| PLA | 30 | 30 | 39.25 | 16.471 | 19.27 | 0.49098 |
| PLA | 30 | 45 | 39.25 | 16.468 | 19.27 | 0.49089 |
| PLA | 30 | 60 | 39.25 | 16.474 | 19.27 | 0.49107 |
| PLA | 30 | 90 | 39.25 | 16.438 | 19.23 | 0.49000 |
| TPU | 30 | 0 | 39.25 | 15.746 | 19.21 | 0.48943 |
| TPU | 30 | 30 | 39.25 | 16.471 | 20.09 | 0.51196 |
| TPU | 30 | 45 | 39.25 | 16.468 | 20.09 | 0.51187 |
| TPU | 30 | 60 | 39.25 | 16.474 | 20.10 | 0.51206 |
| TPU | 30 | 90 | 39.25 | 16.438 | 20.05 | 0.51094 |
| ABS | 50 | 0 | 39.25 | 22.984 | 25.74 | 0.65585 |
| ABS | 50 | 30 | 39.25 | 22.981 | 25.74 | 0.65576 |
| ABS | 50 | 45 | 39.25 | 22.984 | 25.74 | 0.65585 |
| ABS | 50 | 60 | 39.25 | 22.983 | 25.74 | 0.65582 |
| ABS | 50 | 90 | 39.25 | 22.983 | 25.74 | 0.65582 |
| PLA | 50 | 0 | 39.25 | 22.984 | 26.89 | 0.68513 |
| PLA | 50 | 30 | 39.25 | 22.981 | 26.89 | 0.68504 |
| PLA | 50 | 45 | 39.25 | 22.984 | 26.89 | 0.68513 |
| PLA | 50 | 60 | 39.25 | 22.983 | 26.89 | 0.68510 |
| PLA | 50 | 90 | 39.25 | 22.983 | 26.89 | 0.68510 |
| TPU | 50 | 0 | 39.25 | 22.984 | 28.04 | 0.71441 |
| TPU | 50 | 30 | 39.25 | 22.981 | 28.04 | 0.71431 |
| TPU | 50 | 45 | 39.25 | 22.984 | 28.04 | 0.71441 |
| TPU | 50 | 60 | 39.25 | 22.983 | 28.04 | 0.71438 |
| TPU | 50 | 90 | 39.25 | 22.983 | 28.04 | 0.71438 |
| ABS | 70 | 0 | 39.25 | 28.815 | 32.27 | 0.82224 |
| ABS | 70 | 30 | 39.25 | 29.498 | 33.04 | 0.84173 |
| ABS | 70 | 45 | 39.25 | 29.497 | 33.04 | 0.84170 |
| ABS | 70 | 60 | 39.25 | 29.497 | 33.04 | 0.84170 |
| ABS | 70 | 90 | 39.25 | 29.483 | 33.02 | 0.84130 |
| PLA | 70 | 0 | 39.25 | 28.815 | 33.71 | 0.85894 |
| PLA | 70 | 30 | 39.25 | 29.498 | 34.51 | 0.87930 |
| PLA | 70 | 45 | 39.25 | 29.497 | 34.51 | 0.87927 |
| PLA | 70 | 60 | 39.25 | 29.497 | 34.51 | 0.87927 |
| PLA | 70 | 90 | 39.25 | 29.483 | 34.50 | 0.87886 |
| TPU | 70 | 0 | 39.25 | 28.815 | 35.15 | 0.89565 |
| TPU | 70 | 30 | 39.25 | 29.498 | 35.99 | 0.91688 |
| TPU | 70 | 45 | 39.25 | 29.497 | 35.99 | 0.91685 |
| TPU | 70 | 60 | 39.25 | 29.497 | 35.99 | 0.91685 |
| TPU | 70 | 90 | 39.25 | 29.483 | 35.97 | 0.91641 |
| ABS | 90 | 0 | 39.25 | 35.651 | 39.93 | 1.01730 |
| ABS | 90 | 30 | 39.25 | 36.013 | 40.33 | 1.02763 |
| ABS | 90 | 45 | 39.25 | 36.013 | 40.33 | 1.02763 |
| ABS | 90 | 60 | 39.25 | 36.013 | 40.33 | 1.02763 |
| ABS | 90 | 90 | 39.25 | 36.011 | 40.33 | 1.02758 |
| PLA | 90 | 0 | 39.25 | 35.651 | 41.71 | 1.06272 |
| PLA | 90 | 30 | 39.25 | 36.013 | 42.14 | 1.07351 |
| PLA | 90 | 45 | 39.25 | 36.013 | 42.14 | 1.07351 |
| PLA | 90 | 60 | 39.25 | 36.013 | 42.14 | 1.07351 |

**Table 4.** *Cont.*

| Material | Infill Density | Infill Phase Angle | Theoretical Volume with Airgap, $cm^3$ | Theoretical Volume of Infill, $cm^3$ | Theoretical Mass, g | Theoretical Density, $g/cm^3$ |
|---|---|---|---|---|---|---|
| PLA | 90 | 90 | 39.25 | 36.011 | 42.13 | 1.07345 |
| TPU | 90 | 0 | 39.25 | 35.651 | 43.49 | 1.10813 |
| TPU | 90 | 30 | 39.25 | 36.013 | 43.94 | 1.11938 |
| TPU | 90 | 45 | 39.25 | 36.013 | 43.94 | 1.11938 |
| TPU | 90 | 60 | 39.25 | 36.013 | 43.94 | 1.11938 |
| TPU | 90 | 90 | 39.25 | 36.011 | 43.93 | 1.11932 |

At lower photon energies, the probability of interactions, such as the photoelectric effect or Compton scattering, is higher, resulting in greater attenuation. However, as photon energy increases, these interaction probabilities decrease, which is reflected in the observed reduction in attenuation coefficients. This trend is typical for materials used in radiation shielding and imaging, as higher-energy photons have enough energy to pass through the material with fewer interactions. Understanding this behavior is essential for designing materials and structures that can effectively modulate radiation exposure in medical and industrial applications (Figure 3).

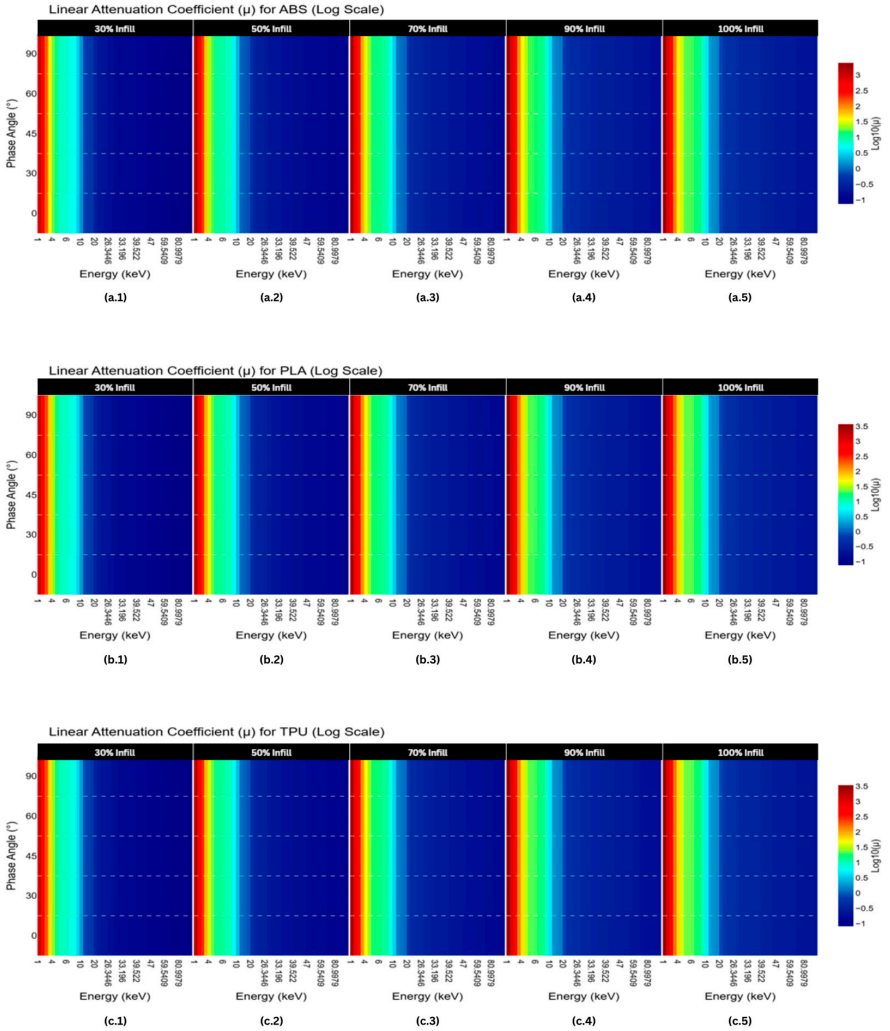



**Figure 3.** Linear attenuation coefficient heatmap on phase angle vs. energy graphs of (**a.1**–**a.5**) ABS, (**b.1**–**b.5**) PLA, and (**c.1**–**c.5**) TPU in increasing infill densities.

The observed dependence of attenuation on infill density can be physically interpreted as a combined effect of the polymer's intrinsic density, molecular structure, and the effective bulk density created by the infill architecture. PLA ($(C_3H_4O_2)_n$) and ABS ($(C_8H_8 \cdot C_4H_6 \cdot C_3H_3N)_n$) are both rigid, amorphous thermoplastics with relatively lower mass densities compared to TPU, whose repeating unit ($(C_3H_8N_2O)_n$) contains flexible, phase-segregated soft and hard segments. These segments increase chain packing efficiency and contribute to TPU's higher effective density. Since attenuation in the diagnostic X-ray range is primarily governed by photoelectric absorption and Compton scattering—both of which scale with electron density—the elemental composition of each polymer becomes relevant. The higher proportion of heavier atoms (e.g., nitrogen and oxygen) in TPU increases its average atomic number and electron concentration, resulting in stronger photon interaction cross sections and therefore higher attenuation. The chemical formulas of ABS, PLA, and TPU were used in the calculations to quantify these compositional differences [16,18,31,32].

Infill density modulates the "effective density" of the printed part, and thus its attenuation coefficient, by adjusting the fraction of material relative to air. As air gaps are reduced, the continuous material pathways increase the average electron density along the photon path, resulting in higher attenuation. This explains the consistent trend observed across all polymers: denser infill geometries behave increasingly like solid masses of polymer, whereas sparse infill patterns introduce lower-density regions that reduce photon interactions [31].

Across all materials tested, consistent patterns were observed; see Figure 4. The median values and the interquartile range (IQR) remained stable, even with variations in infill densities. As expected, the materials showed the highest median values at 100% infill density. While there were some outliers and variations (represented by the whiskers), most data points clustered around consistent values, reflecting reliable trends.

Interestingly, there was a slight increase in the median as infill density increased, particularly at 100%. This suggests that infill density has a noticeable, though moderate, effect on the attenuation coefficient. However, the phase angle did not appear to cause significant changes in the distribution of values. This may be due to the fact that the software calculations were primarily based on material densities and atomic concentrations, leaving other variables, like phase angles, with limited impact.

To rigorously assess the data, a Kruskal–Wallis Test was applied to determine the statistical significance of the differences in attenuation across the materials, given the set parameters. The results of the test supported the initial observations from Figure 4, where an increase in infill density was associated with enhanced attenuation. This was confirmed by a $p$-value of less than 0.05, indicating a statistically significant effect of infill density on attenuation (Table 5). Conversely, variations in phase angle did not yield statistically significant differences, as the $p$-value exceeded the 0.05 threshold. This finding aligns with the earlier discussion in Figure 4, reinforcing the conclusion that phase angle has a negligible effect on attenuation under the conditions examined in this study, which was summarized in Figure 5.

The inclusion of phase angle as a parameter in this study was originally motivated by the theoretical expectation that altering the thickness of the material could modulate the effective photon pathlength. In Beer–Lambert's Law, attenuation is highly dependent on the material, pathlength and the ratio of incident to transmitted photon intensity. With this, introducing small air gaps to decrease the bulk density of the material could alter the attenuating property of the material.

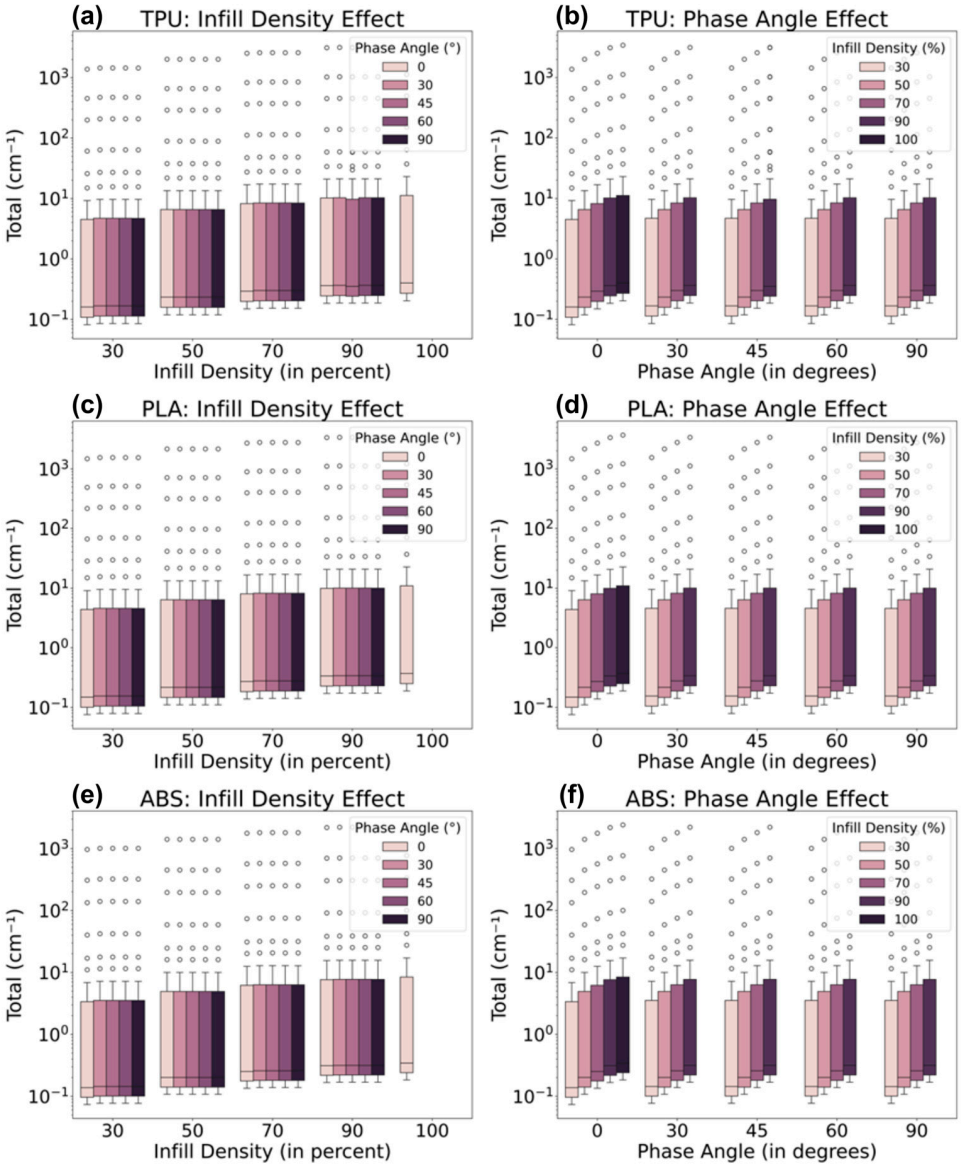



**Figure 4.** Effect of infill density at constant phase angle and effect of phase angle at constant infill density plots of (**a**,**b**) ABS, (**c**,**d**) PLA, and (**e**,**f**) TPU.

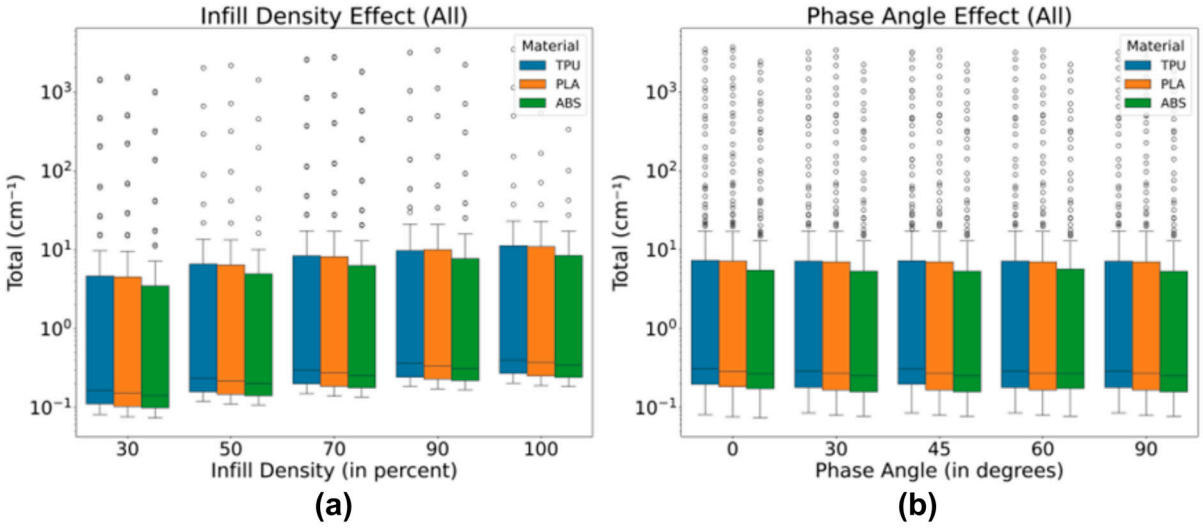



**Figure 5.** Effect of (**a**) varying infill densities and (**b**) phase angle for different materials.

https://doi.org/10.3390/polym18010049

**Table 5.** Kruskal–Wallis Test Results for varying infill density and phase angle.

| **Varying Infill Density at Constant Phase Angle** | | | |
|---|---|---|---|
| **Material** | **Phase Angle, (°)** | ***p*-Value** | **Statistical Significance** |
| ABS | 0 | 0.000184 | Yes |
| ABS | 30 | 0.001226 | Yes |
| ABS | 45 | 0.001219 | Yes |
| ABS | 60 | 0.000199 | Yes |
| ABS | 90 | 0.001226 | Yes |
| PLA | 0 | 0.000431 | Yes |
| PLA | 30 | 0.002435 | Yes |
| PLA | 45 | 0.002435 | Yes |
| PLA | 60 | 0.002435 | Yes |
| PLA | 90 | 0.002406 | Yes |
| TPU | 0 | 0.000420 | Yes |
| TPU | 30 | 0.002388 | Yes |
| TPU | 45 | 0.000567 | Yes |
| TPU | 60 | 0.002377 | Yes |
| TPU | 90 | 0.002350 | Yes |
| **Varying Phase Angle at Constant Infill Density** | | | |
| **Material** | **Infill Density, %** | ***p*-Value** | **Statistical Significance** |
| ABS | 30 | 0.986465 | No |
| ABS | 50 | 0.998844 | No |
| ABS | 70 | 0.994958 | No |
| ABS | 90 | 0.996336 | No |
| PLA | 30 | 0.987389 | No |
| PLA | 50 | 0.998844 | No |
| PLA | 70 | 0.995209 | No |
| PLA | 90 | 0.997087 | No |
| TPU | 30 | 0.987771 | No |
| TPU | 50 | 0.998844 | No |
| TPU | 70 | 0.994958 | No |
| TPU | 90 | 0.991924 | No |

However, the attenuation coefficients used in this work were derived using the EpiXS software, which calculates attenuation solely from homogenized bulk parameters such as density, elemental composition, and percent composition. EpiXS does not incorporate geometric, spatial, or directional information from the infill architecture and therefore cannot model potential microstructural orientation-dependent effects. The null result regarding phase angle must thus be interpreted as a computational limitation rather than evidence that the cross-section of attenuating material has no physical impact on photon interactions.

Three considerations clarify this outcome:

(1) EpiXS assumes macroscopic uniformity and cannot simulate geometric orientation effects;
(2) Any real-world pathlength or anisotropy effects are below the sensitivity of the homogenized model; and
(3) High-fidelity Monte Carlo simulations or physical measurements were beyond the scope of this study.

Therefore, the apparent insignificance of phase angle reflects modeling constraints rather than definitive physical behavior. Future work—including planned experimental validation—will evaluate whether infill orientation contributes measurable differences in attenuation for real 3D-printed structures.

Among the three materials, TPU consistently exhibited higher linear attenuation coefficient values across both varying infill densities and phase angles. This can be attributed to its higher intrinsic density and greater atomic concentration compared to the other materials. These material properties contribute to TPU's superior attenuation capabilities, allowing it to block more radiation than the other tested polymers. In addition to its bulk density advantage, TPU's enhanced attenuation performance also means that Compton scattering becomes the dominant interaction mechanism and depends largely on electron density. TPU's higher mass density, therefore, also increases scattering-based attenuation compared to PLA and ABS [33–37].

The calculated attenuation coefficients fall within the general range reported in prior studies on 3D-printed phantoms, although direct comparisons must account for differences in material composition, print geometry, and measurement energy. Santos et al. [38] reported similar attenuation behavior for PLA phantoms, noting that attenuation increased proportionally with infill density; the PLA values follow the same trend, though our coefficients are slightly higher due to differences in filament formulation and effective density. Savi et al. [39] demonstrated that ABS phantoms typically yield lower attenuation than PLA, a trend also mirrored in our results, where ABS consistently produced the lowest coefficients among the three tested materials. Meanwhile, Kairn et al. [40] emphasized the strong sensitivity of attenuation to print density rather than material type; our findings agree with this conclusion, but the wider material comparison shows that intrinsic polymer density introduces additional variation not explored in those earlier studies. Taken together, the comparison suggests that the geometry-based approach is consistent with established behavior while extending the literature by incorporating a broader material set and a more controlled analysis of infill-driven density effects.

The three materials demonstrated a linear relationship between infill densities and linear attenuation coefficients, as illustrated in Figure 6. Among the polymers, TPU exhibited the greatest sensitivity to changes in infill densities, with a slope of 1.1194, while ABS displayed the least sensitivity, with a slope of 0.7257. This suggests that TPU is the most compatible material for radiation shielding applications, particularly in contexts requiring a flexible interface, given its higher flexibility compared to the other two polymers. Furthermore, the data for all materials showed an excellent linear fit, indicating that interpolation for material design and modulation of attenuation is highly reliable.

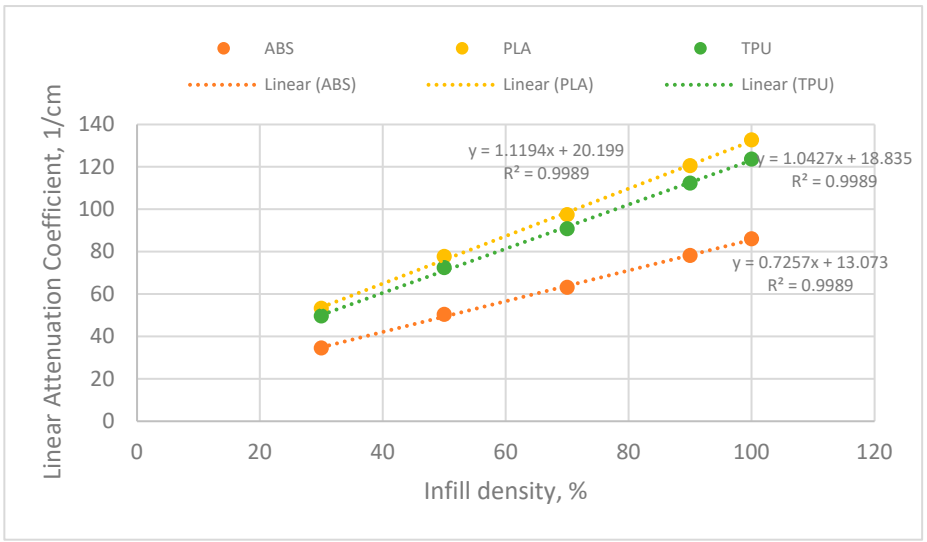



**Figure 6.** Linear regression analysis of different materials in varying infill densities.

When extrapolating to lower infill densities, TPU exhibited the highest baseline attenuation coefficient at 20.199 $cm^{-1}$, followed by PLA at 18.835 $cm^{-1}$ and ABS at 13.073 $cm^{-1}$. These results indicate that even at lower infill densities, such as 30%, TPU maintains effective radiation attenuation properties. PLA, with a relatively small difference from TPU, presents a viable alternative, particularly in situations where a stiffer and more cost-effective material is needed compared to TPU or ABS.

Unlike state-of-the-art studies that rely heavily on metal- or ceramic-filled composite filaments (e.g., tungsten-infused [41], bismuth-infused [41], or lead-infused [11] polymers), our approach demonstrates that meaningful attenuation modulation can be achieved purely through geometric control using standard, commercially available polymers. Filler-based composites increase attenuation by enhancing the atomic number (Z) of the bulk material, but these materials are more expensive, harder to print, and often suffer from poor layer adhesion and inhomogeneous particle distribution. In contrast, this method leverages infill density, patterning, and controlled airgap distribution to shape the effective density of the printed structure without modifying the material composition. This geometry-based modulation provides a low-cost and lightweight alternative for customizable shielding designs, particularly useful where flexibility, biocompatibility, or weight constraints make high-Z composites impractical.

## 4. Conclusions

This study successfully demonstrated the potential of varying infill densities and phase angles in 3D-printed ABS, PLA, and TPU materials for radiation attenuation applications in the X-ray region. TPU exhibited the highest responsiveness to changes in infill density, with a slope of 1.1194, significantly outperforming ABS (slope of 0.7257) and PLA (slope of 0.9251). The baseline attenuation coefficient for TPU at 30% infill density was the highest at 20.199 $cm^{-1}$, compared to 18.835 $cm^{-1}$ for PLA and 13.073 $cm^{-1}$ for ABS. This indicates that TPU is particularly suited for radiation shielding, especially in applications requiring flexible materials.

The statistical analysis, using the Kruskal–Wallis test, confirmed the significant impact of infill density on attenuation, with $p$-values less than 0.05 across all materials. In contrast, phase angle did not significantly affect attenuation, with $p$-values exceeding 0.05, suggesting that phase angle is a parameter that cannot be directly simulated using the EpiXS program. These results highlight the importance of infill density as a key parameter in designing radiation protection materials. The use of a simple rectangular infill with phase-angle variation was intentional, allowing this study to isolate geometric orientation effects under controlled conditions. Because EpiXS treats materials as homogenized media, orientation-dependent microstructural effects could not be captured, which explains the observed phase-angle insensitivity. This result should not be generalized to more complex infill geometries such as gyroid or honeycomb, where curvature and anisotropy may influence photon transport. The present work, therefore, establishes a necessary baseline for future studies, which will evaluate advanced infill patterns and incorporate physical measurements or Monte Carlo simulations to capture geometry-dependent attenuation effects.

While ABS, PLA, and TPU are not traditional high-Z shielding materials, this study demonstrates their applicability in low-energy diagnostic radiation environments due to their lightweight nature, ease of fabrication, and adaptability through infill manipulation. Their intrinsic material differences—such as density and molecular structure—also help explain their varying attenuation behaviors. PLA, with its relatively higher density and oxygen-rich molecular composition, showed slightly greater attenuation than ABS. TPU provided the highest attenuation in this study, likely due to its unique urethane-based

structure and how it responds to infill variation. These observations confirm that polymer composition can meaningfully influence X-ray attenuation, particularly when paired with geometric optimization via additive manufacturing.

Additionally, TPU's superior attenuation properties even at lower infill densities, along with PLA's comparable performance at a slightly lower attenuation (18.835 $cm^{-1}$ at 30% infill), make them excellent candidates for radiation-shielding applications. PLA, being a stiffer yet cost-effective alternative to TPU, can also be used in cases where higher rigidity is required without compromising too much on radiation protection, whereas TPU offers advantages for ergonomic, flexible applications. ABS, with moderate attenuation characteristics, remains viable for situations where structural strength and ease of processing are prioritized. With the advantages of TPU in the attenuation modulation effect, this material is a potential candidate in manufacturing patient-specific boluses for radiotherapy applications. The flexibility of TPU is advantageous as it reduces the risk of air gaps between the bolus and the patient's skin, which is a critical factor in ensuring uniform dose delivery to superficial tumor sites.

As a critical next step, future work will focus on experimentally validating the simulation results using a controlled X-ray imaging setup. This validation will involve fabricating test phantoms with specified infill densities and phase angles and measuring their attenuation under clinical or diagnostic energy ranges. Comparing experimental transmission values with the predicted linear attenuation coefficients will allow for calibration of the calculation model, verification of material behavior in real-world conditions, and refinement of design parameters. Such experimental confirmation is essential to establish the practical applicability of 3D-printed polymers for radiation shielding and to guide the development of optimized protective devices.

The integration of additive manufacturing in producing custom-designed radiation protection gear offers significant improvements in the accessibility, performance, and comfort of protective equipment in both medical and industrial contexts. These findings lay a strong foundation for future work, which can explore more complex infill geometries and phase angle combinations, as well as testing under different radiation spectra, to further optimize material design for radiation shielding.

## 5. Patents

The utility model application will be filed in 2026 under the Philippine Intellectual Property Office.

**Author Contributions:** Conceptualization, T.B.L. and J.H.C.; methodology, T.B.L., J.H.C. and M.J.A.; software, T.B.L. and A.A.; validation, T.B.L., J.H.C. and A.A.; formal analysis, T.B.L., J.H.C. and A.A.; investigation, T.B.L., J.H.C., E.A., M.L.A., R.J.W.L., G.B.F. and P.M.; resources, T.B.L., E.A., G.N.S. and A.A.; data curation, T.B.L., J.H.C. and E.A.; writing—original draft preparation, T.B.L., J.H.C., M.L.A., R.J.W.L. and G.B.F.; writing—review and editing, T.B.L., J.H.C., E.A., M.L.A., R.J.W.L., G.B.F., P.M., G.N.S., A.A., R.A. and M.J.A.; visualization, T.B.L., J.H.C. and E.A.; supervision, G.N.S., A.A. and R.A.; project administration, T.B.L. and J.H.C.; funding acquisition, T.B.L. and J.H.C. All authors have read and agreed to the published version of the manuscript.

**Funding:** This research was supported by the Department of Science and Technology (DOST) under the DOST-Grants in Aid Project No. 11233 under DOST-PCIEERD as a granting agency. The APC was funded by the same project headed by Engr. Fred P. Liza of DOST—Metals Industry Research and Development Center.

**Institutional Review Board Statement:** Not applicable for this study due to non-involvement of humans or animals.

**Data Availability Statement:** The raw data supporting the conclusions of this article will be made available by the authors on request.

**Acknowledgments:** The authors would like to thank Fred P. Liza for providing the financial assistance through his approved project and for reviewing the paper. Additionally, the authors would like to express their gratitude to Karl Albright Tiston in providing the graphical representation of the polymer structures which were included in Table 2. During the preparation of this work, the author TBG Lopez used ChatGPT version GPT-5.0 to check grammar, tense consistency, and flow of discussion. After using this tool, the author reviewed and edited the content as needed and took full responsibility for the content of the publication.

**Conflicts of Interest:** Author Michael Joe S. Alvarez was employed by the company St. Elizabeth Hospital, Inc. The remaining authors declare that the research was conducted in the absence of any commercial or financial relationships that could be construed as a potential conflict of interest.

## Abbreviations

The following abbreviations are used in this manuscript:

| | |
|---|---|
| ABS | Acrylonitrile Butadiene Styrene |
| PLA | Polylactic Acid |
| TPU | Thermoplastic Polyurethane |
| CAD | Computer-Aided Design |
| LAC | Linear Attenuation Coefficient |

## References

1. Magrini, S.M.; Pasinetti, N.; Belgioia, L.; Triggiani, L.; Levis, M.; Ricardi, U.; Corvò, R. Applying radiation protection and safety in radiotherapy. *Radiol. Medica* **2019**, *124*, 777–782. [CrossRef]
2. Ploussi, A.; Efstathopoulos, E.P.; Brountzos, E. The Importance of Radiation Protection Education and Training for Medical Professionals of All Specialties. *Cardiovasc. Interv. Radiol.* **2021**, *44*, 829–834. [CrossRef]
3. Kitahara, C.M.; Linet, M.S.; Drozdovitch, V.; Alexander, B.H.; Preston, D.L.; Simon, S.L.; Freedman, D.M.; Brill, A.B.; Miller, J.S.; Little, M.P.; et al. Cancer and circulatory disease risks in US radiologic technologists associated with performing procedures involving radionuclides. *Occup. Environ. Med.* **2015**, *72*, 770–776. [CrossRef]
4. Talley, S.J.; Robison, T.; Long, A.M.; Lee, S.Y.; Brounstein, Z.; Lee, K.-S.; Geller, D.; Lum, E.; Labouriau, A. Flexible 3D printed silicones for gamma and neutron radiation shielding. *Radiat. Phys. Chem.* **2021**, *188*, 109616. [CrossRef]
5. Kharfi, F.; Benkahila, K.; Boulkhessaim, F.; Betka, A.; Meziri, A.; Khelfa, S.; Ghediri, N. Implementation of 3D Printing and Modeling Technologies for the Fabrication of Dose Boluses for External Radiotherapy at the CLCC of Sétif, Algeria. *Technol. Cancer Res. Treat.* **2024**, *23*, 15330338241266479. [CrossRef] [PubMed]
6. MIRA Safety. MIRA Safety HAZ-SUIT Protective CBRN HAZMAT Suit. Available online: https://www.mirasafety.com/products/mira-safety-haz-suit-hazmat-suit?srsltid=AfmBOoqhBKbIQBDdzPsxVIQiR514TNeLpsu4taPO9OZQ__FtPnA4GtOt (accessed on 5 October 2024).
7. More, C.V.; Alsayed, Z.; Badawi, M.S.; Thabet, A.A.; Pawar, P.P. Polymeric composite materials for radiation shielding: A review. *Environ. Chem. Lett.* **2021**, *19*, 2057–2090. [CrossRef] [PubMed]
8. Almisned, G.; Akman, F.; AbuShanab, W.S.; Tekin, H.O.; Kaçal, M.R.; Issa, S.A.M.; Polat, H.; Oltulu, M.; Ene, A.; Zakaly, H.M.H. Novel Cu/Zn Reinforced Polymer Composites: Experimental Characterization for Radiation Protection Efficiency (RPE) and Shielding Properties for Alpha, Proton, Neutron, and Gamma Radiations. *Polymers* **2021**, *13*, 3157. [CrossRef]
9. Mokhtari, K.; Saadi, M.K.; Panahi, H.A.; Jahanfarnia, G. The shielding properties of the ordinary concrete reinforced with innovative nano polymer particles containing PbO–H3BO3 for dual protection against gamma and neutron radiations. *Radiat. Phys. Chem.* **2021**, *189*, 109711. [CrossRef]
10. InFab. Radiation Shielding. Available online: https://infabcorp.com/products/radiation-shielding/ (accessed on 6 July 2023).
11. McCaffrey, J.P.; Shen, H.; Downton, B.; Mainegra-Hing, E. Radiation attenuation by lead and nonlead materials used in radiation shielding garments. *Med. Phys.* **2007**, *34*, 530–537. [CrossRef]
12. Beck, D.; Bickus, J.; Klein, E.; Miller, P.; Di Cecca, S.; Benz, R.; Barney, A.; Longton, R.; Coon, A.; Smith, M.; et al. Additive Manufacturing of Multimaterial Composites for Radiation Shielding and Thermal Management. *ACS Appl. Mater. Interfaces* **2023**, *15*, 35400–35410. [CrossRef] [PubMed]

13. Jakupi, K.; Dukovski, V.; Kočov, A. Analysis of additive manufacturing technology input parameters in manufacturing of bolus. *Mech. Eng. Sci. J.* **2022**, *40*, 17–22. [CrossRef]
14. Diaz-Merchan, J.A.; Martinez-Ovalle, S.A.; Vega-Carrillo, H.R. Development of a 3D printing process of bolus using BolusCM material for radiotherapy with electrons. *Appl. Radiat. Isot.* **2023**, *199*, 110899. [CrossRef]
15. Sands, G.; Clark, C.H.; McGarry, C.K. A review of 3D printing utilisation in radiotherapy in the United Kingdom and Republic of Ireland. *Phys. Medica* **2023**, *115*, 103143. [CrossRef]
16. Ahmed, A.M.M.; Buschmann, M.; Breyer, L.; Kuntner, C.; Homolka, P. Tailoring the Mass Density of 3D Printing Materials for Accurate X-ray Imaging Simulation by Controlled Underfilling for Radiographic Phantoms. *Polymers* **2024**, *16*, 1116. [CrossRef]
17. Okkalidis, F.; Chatzigeorgiou, C.; Okkalidis, N.; Dukov, N.; Milev, M.; Bliznakov, Z.; Mettivier, G.; Russo, P.; Bliznakova, K. Characterization of Commercial and Custom-Made Printing Filament Materials for Computed Tomography Imaging of Radiological Phantoms. *Technologies* **2024**, *12*, 139. [CrossRef]
18. Ma, X.; Buschmann, M.; Unger, E.; Homolka, P. Classification of X-Ray Attenuation Properties of Additive Manufacturing and 3D Printing Materials Using Computed Tomography from 70 to 140 kVp. *Front. Bioeng. Biotechnol.* **2021**, *9*, 763960. [CrossRef] [PubMed]
19. Ciobanu, A.C.; Petcu, L.C.; Járai-Szabó, F.; Bálint, Z. Exploring the impact of filament density on the responsiveness of 3D-Printed bolus materials for high-energy photon radiotherapy. *Phys. Med.* **2024**, *127*, 104849. [CrossRef]
20. Kavun, Y.; Kamer, M.S. Effect of line width and layer height variation on radiation shielding properties of 3D-printed poly(lactic acid) materials. *Radiat. Phys. Chem.* **2026**, *240*, 113410. [CrossRef]
21. Mei, K.; Pasyar, P.; Geagan, M.; Liu, L.P.; Shapira, N.; Gang, G.J.; Stayman, J.W.; Noël, P.B. Design and fabrication of 3D-printed patient-specific soft tissue and bone phantoms for CT imaging. *Sci. Rep.* **2023**, *13*, 17495. [CrossRef] [PubMed]
22. Liao, Y.; Liu, C.; Coppola, B.; Barra, G.; Di Maio, L.; Incarnato, L.; Lafdi, K. Effect of Porosity and Crystallinity on 3D Printed PLA Properties. *Polymers* **2019**, *11*, 1487. [CrossRef] [PubMed]
23. Lee, A.; Wynn, M.; Quigley, L.; Salviato, M.; Zobeiry, N. Effect of temperature history during additive manufacturing on crystalline morphology of PEEK. *Adv. Ind. Manuf. Eng.* **2022**, *4*, 100085. [CrossRef]
24. Xiao, J.; Lei, Y. Enriching Semantics of Geometry Features and Parameters for Additive Manufacturing Peculiar Structure Based on STEP Standards. *Crystals* **2022**, *12*, 1154. [CrossRef]
25. Hila, F.C.; Asuncion-Astronomo, A.; Dingle, C.A.M.; Jecong, J.F.M.; Javier-Hila, A.M.V.; Gili, M.B.Z.; Balderas, C.V.; Lopez, G.E.P.; Guillermo, N.R.D.; Amorsolo, A.V. EpiXS: A Windows-based program for photon attenuation, dosimetry and shielding based on EPICS2017 (ENDF/B-VIII) and EPDL97 (ENDF/B-VI.8). *Radiat. Phys. Chem.* **2021**, *182*, 109331. [CrossRef]
26. Dassault Systèmes—SolidWorks Corporation. Dassault Solidworks. 2020. Available online: https://www.solidworks.com/ (accessed on 12 December 2025).
27. Gregor-Svetec, D. Polymers in printing filaments. In *Polymers for 3D Printing*; Elsevier: Amsterdam, The Netherlands, 2022; pp. 155–269. [CrossRef]
28. Prajapati, S.; Sharma, J.K.; Kumar, S.; Pandey, S.; Pandey, M.K. A review on comparison of physical and mechanical properties of PLA, ABS, TPU, and PETG manufactured engineering components by using fused deposition modelling. *Mater. Today Proc.* 2024; *in press*. [CrossRef]
29. Sardinha, M.; Ferreira, L.; Diogo, H.; Ramos, T.R.P.; Reis, L.; Vaz, M.F. Material extrusion of TPU: Thermal characterization and effects of infill and extrusion temperature on voids, tensile strength and compressive properties. *Rapid Prototyp. J.* **2025**, *31*, 62–81. [CrossRef]
30. Rahmatabadi, D.; Ghasemi, I.; Baniassadi, M.; Abrinia, K.; Baghani, M. 3D printing of PLA-TPU with different component ratios: Fracture toughness, mechanical properties, and morphology. *J. Mater. Res. Technol.* **2022**, *21*, 3970–3981. [CrossRef]
31. Choi, Y.; Jang, Y.J.; Kim, K.B.; Bahng, J.; Choi, S.H. Characterization of Tissue Equivalent Materials Using 3D Printing for Patient-Specific DQA in Radiation Therapy. *Appl. Sci.* **2022**, *12*, 9768. [CrossRef]
32. Tong, H.; Pegues, H.; Samei, E.; Lo, J.Y.; Wiley, B.J. Technical note: Controlling the attenuation of 3D-printed physical phantoms for computed tomography with a single material. *Med. Phys.* **2022**, *49*, 2582–2589. [CrossRef]
33. Sathish, K.; Manjunatha, H.; Vidya, Y.; Sridhar, K.; Seenappa, L.; Reddy, B.C.; Raj, S.A.C.; Gupta, P.D. X-rays/gamma rays radiation shielding properties of Barium–Nickel–Iron oxide nanocomposite synthesized via low temperature solution combustion method. *Radiat. Phys. Chem.* **2022**, *194*, 110053. [CrossRef]
34. Sathish, K.; Sridhar, K.; Seenappa, L.; Manjunatha, H.; Vidya, Y.; Reddy, B.C.; Manjunatha, S.; Santhosh, A.; Munirathnam, R.; Raj, A.C.; et al. X-ray/gamma radiation shielding properties of Aluminium-Barium Zinc Oxide nanoparticles synthesized via low temperature solution combustion method. *Nucl. Eng. Technol.* **2023**, *55*, 1519–1526. [CrossRef]
35. Alshahri, S.; Alsuhybani, M.; Alosime, E.; Almurayshid, M.; Alrwais, A.; Alotaibi, S. LDPE/Bismuth Oxide Nanocomposite: Preparation, Characterization and Application in X-ray Shielding. *Polymers* **2021**, *13*, 3081. [CrossRef]
36. Li, Z.; Zhou, W.; Zhang, X.; Gao, Y.; Guo, S. High-efficiency, flexibility and lead-free X-ray shielding multilayered polymer composites: Layered structure design and shielding mechanism. *Sci. Rep.* **2021**, *11*, 4384. [CrossRef] [PubMed]

37. Aghamiri, M.R.; Mortazavi, S.M.J.; Tayebi, M.; Mosleh-Shirazi, M.A.; Baharvand, H.; Tavakkoli-Golpayegani, A.; Zeinali-Rafsanjani, B. A Novel Design for Production of Efficient Flexible Lead-Free Shields against X-ray Photons in Diagnostic Energy Range. *J. Biomed. Phys. Eng.* **2011**, *1*, 17–21.
38. Santos, J.C.; Almeida, C.D.; Iwahara, A.; Peixoto, J.E. Characterization and applicability of low-density materials for making 3D physical anthropomorphic breast phantoms. *Radiat. Phys. Chem.* **2019**, *164*, 108361. [CrossRef]
39. Savi, M.; Villani, D.; Andrade, M.A.B.; Rodrigues, O.; Potiens, M.P.A. Study on attenuation of 3D printing commercial filaments on standard X-ray beams for dosimetry and tissue equivalence. *Radiat. Phys. Chem.* **2021**, *182*, 109365. [CrossRef]
40. Kairn, T.; Crowe, S.B.; Markwell, T. Use of 3D Printed Materials as Tissue-Equivalent Phantoms. In Proceedings of the World Congress on Medical Physics and Biomedical Engineering, Toronto, ON, Canada, 7–12 June 2015; pp. 728–731. [CrossRef]
41. Wang, B.; Qiu, T.; Yuan, L.; Fang, Q.; Wang, X.; Guo, X.; Zhang, D.; Lai, C.; Wang, Q.; Liu, Y. A comparative study between pure bismuth/tungsten and the bismuth tungsten oxide for flexible shielding of gamma/X rays. *Radiat. Phys. Chem.* **2023**, *208*, 110906. [CrossRef]

**Disclaimer/Publisher's Note:** The statements, opinions and data contained in all publications are solely those of the individual author(s) and contributor(s) and not of MDPI and/or the editor(s). MDPI and/or the editor(s) disclaim responsibility for any injury to people or property resulting from any ideas, methods, instructions or products referred to in the content.